Printed circuit board based modulated retroreflector using three large-area quantum well modulators

Rohit Nair
Michael E. Teitelbaum
Keith W. Goossen
University of Delaware
Department of Electrical and Computer Engineering
140 Evans Hall
Newark, Delaware 19716
E-mail: nair@ece.udel.edu

Abstract. We demonstrate a modulated retroreflector that utilizes large-area multiple quantum well modulators on all three faces of a retroreflector. The large-area devices, fabricated by metalorganic chemical vapor deposition, are characterized in terms of the yield and leakage currents. A yield higher than that achieved previously using devices fabricated by molecular beam epitaxy is observed. The retroreflector module is constructed using a standard FR4 printed circuit board (PCB) technology, thereby simplifying the wiring issue. A high optical contrast ratio of 8.23 dB is observed for a drive of 20 V. A free-standing PCB retroreflector is explored and found to have insufficient angular tolerances (± 0.5 deg). We show that the angular errors in the corner-cube construction can be corrected for using off-the-shelf optical components as opposed to mounting the PCBs on a precision corner cube, as has been done previously.
[DOI: 10.1117/1.3249750]

Subject terms: retroreflectors; optoelectronics; optical communications; geometric optics; quantum wells; lenses.

Paper 090206R received Mar. 23, 2009; revised manuscript received Aug. 3, 2009; accepted for publication Aug. 17, 2009; published online Oct. 20, 2009.

1 Introduction

Modulated retroreflectors (MRRs) have several military and commercial applications which include low-power communication with ultralight air vehicles,[1] space-to-ground optical communication,[2] terrestrial point-to-point free space optical communication,[3] remote telemetry,[4] remote sensing of hazmats,[5] distance measurement,[6] dynamic optical tags for equipment and personnel,[7] and potentially, on-road vehicle-to-vehicle communication for accident prevention.[8] For communication applications, MRRs can have advantages over radio links in terms of power dissipation and selectivity. The applications listed and others require the construction of 3-D optics and electronics with optical precision.[9]

In the past, there have been several approaches to build MRRs. Microelectromechanical (MEMS) elements such as deformable mirrors,[4] variable etalons,[10,11] or deformable gratings[12] have been used as the modulating element where the MEMS component is basically one of the faces of the corner cube. Another general approach is to use some type of shutter as the aperture of the corner cube such as a ferro liquid crystal.[13] Semiconductor modulators can be also be used as the MRR shutter.[1] The semiconductor modulators are typically in the form of p-i-n diodes where the intrinsic region consists of multiple quantum wells (MQWs). MQW devices exploit the quantum confined Stark effect (QCSE) and are efficient electroabsorption modulators.[14] The semiconductor devices can offer higher bandwidth and angular tolerances than MEMS devices, and can be operated at lower bias voltages. Additionally, they can also be operated as efficient photodetectors, thereby enabling a bidirectional optical link.

In Ref. 1, a transmission-mode MQW modulator was placed at the aperture of a precision milled retroreflector. Such a setup may have reliability issues, since the MQW substrate is free standing and may be highly prone to damage, especially in some military applications. In this work, we consider using three large-area MQW devices on the three faces of the corner cube. We use well-developed microelectronic packaging technology to assemble the module. The MQW devices can be mounted on standard FR4 printed circuit boards (PCBs) and assembled together so that there are modulators on all three faces of the retroreflector. The advantage of using PCBs is that it is easier to provide electrical connections to bias the devices, since tracing metal lines on FR4 boards is a well developed process. Additionally, the boards provide mechanical strength to the brittle device substrates. While based on earlier work, it is possible to simply mount the PCBs on a precision corner cube (as was done in Ref. 4 on a single face); here, a free-standing PCB corner cube structure is explored. We find angular tolerances of ± 0.5 deg in the free-standing PCB corner cube, insufficient for retrocommunication over large distances. We show that if a free-standing PCB corner cube modulator is desired to avoid deleterious issues of needing a precision milled retroreflector, the misalignment can be corrected with front optics.

This approach enables the use of modulators on all three faces, as shown in the schematic in Fig. 1, so a higher contrast ratio (CR) can be achieved. The design and characterization of the large-area MQW devices used in this

0091-3286/2009/$25.00 © 2009 SPIE

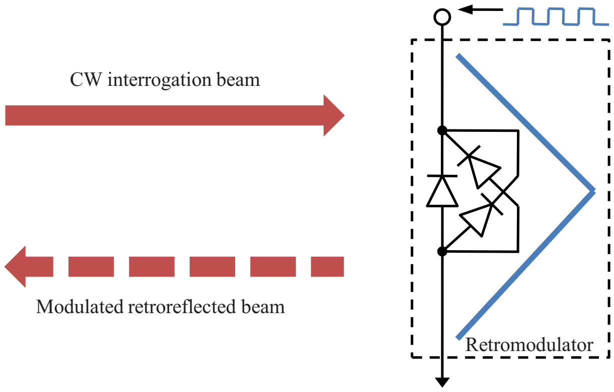

Fig. 1 Schematic showing the MQW diode configuration in the modulated retroreflector. The three diodes are connected in parallel.

work is described in the next section. The construction and the experimental demonstration of the PCB-based MRR is discussed in Sec. 3. This is followed by a section that discusses the effects of the angular misalignment of the retroreflector faces. The design and demonstration of corrective optics to compensate for angular errors is discussed in Sec. 5.

2 Large-Area Multiple Quantum Well Devices

The quantum well devices used in this work are designed to operate at around 1.55 μm. The yield of GaAs-based modulators operating at 0.85 μm can be high.[15] But since the application targeted here involves free space optical propagation, the longer wavelength InP-based devices are chosen for eye safety. Additionally, there is a relatively low loss window in the optical transmission characteristics of the atmosphere around 1.55 μm. The 2-in. wafer with layer structure shown in Fig. 2 was grown by metalorganic chemical vapor deposition (MOCVD) by IQE Incorporated, Bethlehem, Pennsylvania. The intrinsic region of the p-i-n diode consists of 150 85 Å InGaAs wells separated by 35 Å InAlAs barriers lattice matched to InP. The p-i-n layers were grown on an n-type InP substrate. Ti-Au (150 Å/2000 Å) contacts were deposited by evaporation and lift-off to form the top contacts of the devices. The device mesas, with dimensions 3.3 $\times$ 3.3 mm, were created by etching 1 μm into the substrate. A silicon monoxide antireflective coating was deposited on the optical window of the devices using lift-off. A 2000 Å silver film was evaporated on the backside of the wafer to enable the use of the MQW devices in reflection mode, and also to provide the bottom electrical contact. Finally, the individual large-

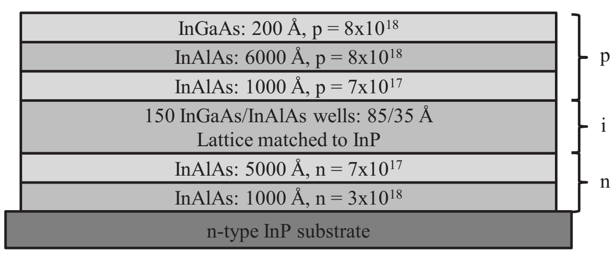

Fig. 2 Layer structure of the MQW modulator.

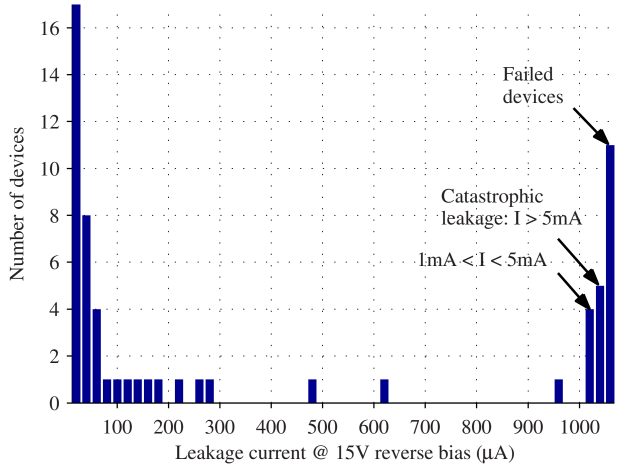

Fig. 3 Leakage current distribution of fabricated MQW diodes with a 15-V reverse bias.

area devices were diced apart. A device face size of 3.3 $\times$ 3.3 mm corresponds to a retroreflector with full width half maximum (FWHM) field of view (FOV) of about 37 deg.

2.1 *Device Yield*

Yield is an important parameter to be considered during device fabrication. A total of 61 large-area quantum well devices were fabricated. The leakage currents for all the devices were measured and the distribution is shown in Fig. 3. About 62% of the devices show excellent diode characteristics and have leakage currents below 300 μA at a reverse bias of 15 V. At this bias, we observed catastrophic leakage currents of 5 mA in 26% of the device. Hence, the area defect density was calculated to be 2.4 defects/cm^2. Here, the defect density is calculated based on the number of working devices out of all the devices fabricated. The defect density observed here is less than that achieved with similar large-area devices fabricated using molecular beam epitaxy (MBE).[16] In the literature, InP-based heterojunction bipolar transistor (HBT) and high electron mobility transistor (HEMT) devices fabricated using MBE[17] and MOCVD[18] on 4-in. wafers show comparable defect densities ($<$50 defects/cm^2). As shown in Fig. 3, some of the MQW diodes had leakage currents between 100 μA and 1 mA. The usability of these devices will depend on the power specifications and heat sinking capabilities of the intended application.

The overall cost of the system depends on the device yield. A high yield is, therefore, desirable. One method to improve the yield is to pixellate a large-area device into several smaller individually addressable devices while keeping the active area high.[19] Pixellation has an added advantage. The use of large-area MQW devices limits its dynamic performance due to its RC limit. The devices fabricated have a capacitance of about 500 pF. Thus, by pixellation, the capacitance of the device can be reduced significantly, thereby enabling higher modulation rates. The device yield can also be further improved by using defectectomy,[20] which is a contactless maskless photolithography process to locate, isolate, and etch away defects.

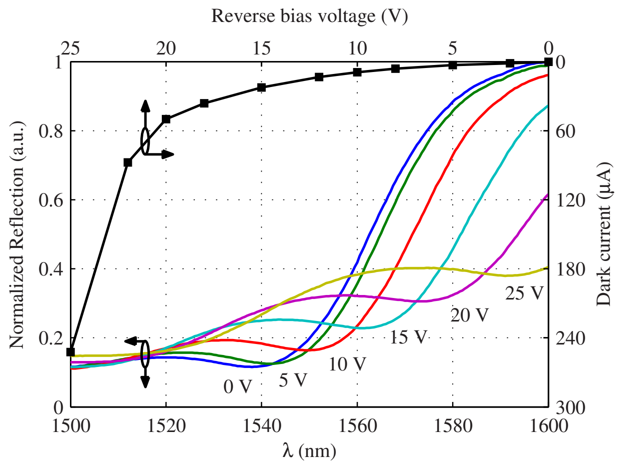

Fig. 4 Modulator reflection spectra for a 0 to 25-V reverse bias with the device tilted at ∼35 deg to the optical axis. Also shown is the diode reverse bias I-V curve.

2.2 *Multiple Quantum Well Diode Electrical and Optical Characteristics*

In applications where a set of MRRs are used along with a laser to enable a bidirectional free-space optical communication link, a low dark current is desired to have high receiver sensitivity. The reverse bias I-V characteristics of one of the fabricated MQW diodes is shown in Fig. 4. At a reverse bias of 20 V, the dark current I_{Dark} is less than 50 μA, which corresponds to a static power dissipation ($P_{S|D}$) of 3 mW per MRR module. Also shown in Fig. 4 is the reflection spectrum of the device at varying reverse bias voltages. The measurement was done with the device tilted at about 35 deg to the optical axis, since in the MRR module the light will always be incident on the device at an oblique angle. The measured reflection contrasts for the device are shown in Fig. 5. A maximum reflection contrast of 4.36 dB is observed with a reverse bias of 20 V at $\lambda = 1579$ nm. A low insertion loss of 0.614 dB is observed. Similarly, at lower reverse bias voltages of 10 and 15 V, reflection contrasts of 2.56 and 4.12 dB are observed at wavelengths 1560.5 and 1569 nm, respectively. With the triple-modulator retroreflector configuration, the system can potentially deliver a total of 7.68, 12.36, and 13.08 dB contrast ratios at 10, 15, and 20 V, respectively. Hence, depending on the $P_{S|D}$-CR trade-off specifications for a given application, an appropriate operating voltage can be used.

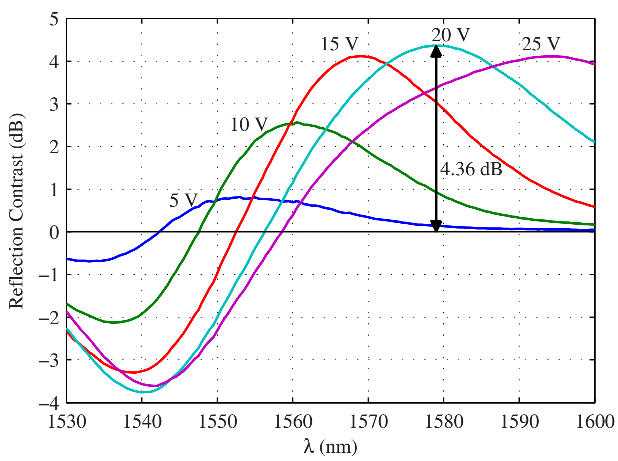

Fig. 5 Modulator reflection contrast for a 0 to 25-V reverse bias. A maximum of 4.36 dB is observed at $\lambda = 1579$ nm for a reverse bias of 20 V.

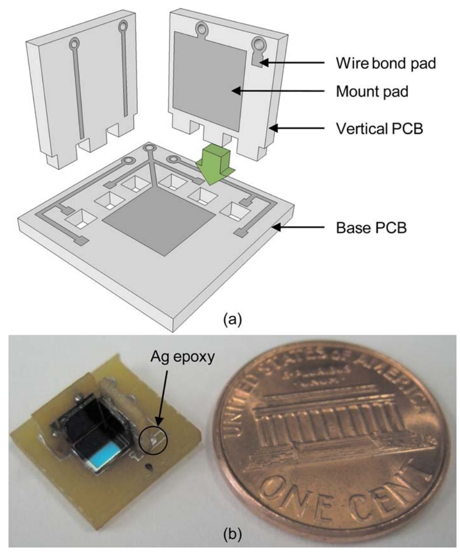

Fig. 6 (a) Pronged PCB schematic. The vertical board on the left is rotated by 180 deg to illustrate the back side metal traces. (b) The PCB-based modulated retroreflector module with the MQW devices die bonded on the boards.

3 Printed Circuit Board Based Modulated Retroreflector

Standard FR4 printed circuit boards can be used to build the MRR module. The schematic of the module is shown in Fig. 6(a). Fingers were milled on the vertical PCBs using a standard tabletop mill. Machining was done so that the vertical PCB fit tightly into the base PCB. The individual large-area MQW modulators were bonded on the metal mounting pad using the electrically conductive epoxy, EPO-TEK® H20E, from Epoxy Technology (Billerica, Massachusetts). After curing the epoxy at about 80 °C for 15 min, the top metal contact of the MQW modulators were wire bonded to the PCB bond pad. The module was then assembled together. The silver epoxy was again used to connect the metal traces on the back side vertical PCB to the pads on the base PCB. The final assembled module is shown in Fig. 6(b).

The assembled MRR was tested using the setup shown in Fig. 7. A continuous wave (cw) tunable laser was used to

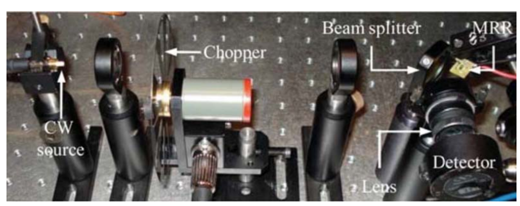

Fig. 7 Modulated retroreflector experimental setup.

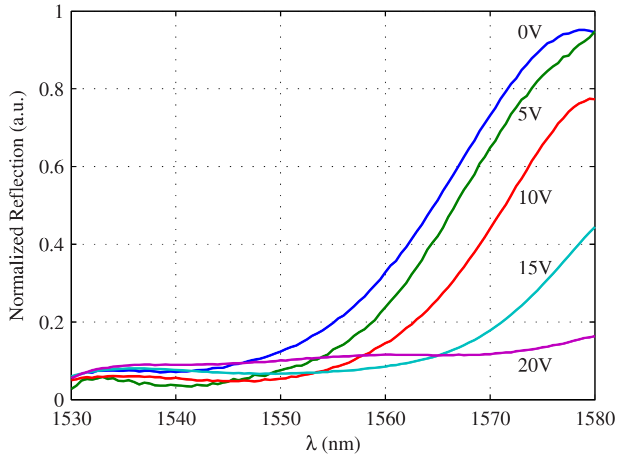

Fig. 8 Modulated retroreflector retroreflection spectra for reverse bias 0 to 20 V.

interrogate the MRR with the source wavelength varying from 1530 to 1580 nm. A beamsplitter was used to redirect the retroreflected beam to a photodetector. The retroreflected photocurrent was measured using a lock-in amplifier with the chopper frequency being the reference.

The measured reflection spectra for bias voltages of 0 to 20 V are shown in Fig. 8, and the corresponding reflection contrast is shown in Fig. 9. With a reverse bias of 20 V, a CR of about 7:1 is observed at a wavelength $\lambda = 1574$ nm. This is a higher CR than that measured by Gilbreath et al.[1] The excitonic absorption peaks of the individual device during preassembly occurred at different wavelengths. This may be the reason for a lower MRR-CR than the expected value of ~13 dB (at 20 V). The power consumption of the MRR is directly proportional to the square of the driving voltage.[1] Thus, for a given CR, the system proposed here dissipates lesser power. This fact is especially important for power-scarce applications.

4 Effects of Angular Misalignment

To study the angular tolerances of the free-standing PCB retromodulator, several modules were assembled with plane

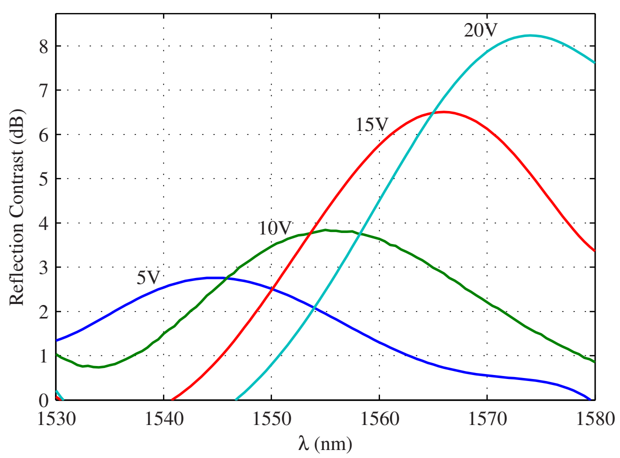

Fig. 9 Modulated retroreflector reflection contrast. A maximum contrast of 8.23 dB is observed at $\lambda = 1574$ nm with a bias of 20 V.

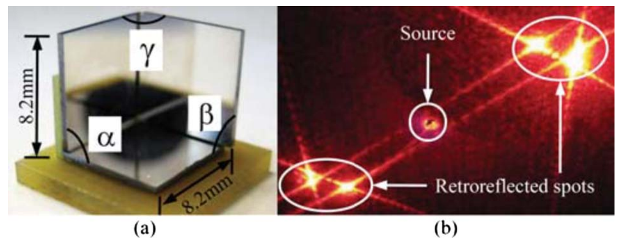

Fig. 10 (a) Assembled corner-cube module with silver mirrors mounted on all three faces. The angles between the faces, α, β and γ, are indicated. (b) Result of illuminating the imperfect retroreflector from a distance of 2.5 m. The shown observation plane is located just in front of the source. No light is retroreflected to the center of the observation plane.

silver mirrors on the three faces, such as the one shown in Fig. 10(a), to measure the angles between the faces. The mirrors were mounted on the three faces using the low viscosity epoxy Tra-Bond 931-1 from Tra-Con, Incorporated, Bedford, Massachusetts. This epoxy was chosen as the adhesive so that it flows evenly between the mount pad and the mirror during the curing process to minimize its contribution to the angular error. In a typical sample, the angle between the two vertical faces γ was measured to be 90 deg. However, the angles between the two vertical PCBs and the base, α and β, were both 89.5 deg. This 0.5 deg deviation has a detrimental effect on the performance of the retroreflector. This "imperfect" retroreflector (IRR) was illuminated using a HeNe laser from a distance of about 2.5 m. As shown in Fig. 10(b), the angular imperfections in the retroreflector results in multiple spots on the observation plane all of which are diverging away from the optical axis. There are multiple retroreflected spots on the observation plane in Fig. 10(b) because the interrogation beam illuminates all three faces of the corner cube simultaneously, resulting in multiple retroreflection pathways.

In general, we observed that we could limit the face angular error to ±0.5 deg in the free-standing FR4 corner cubes. While a solution, as shown earlier for a single modulated facet, is to mount the PCB directly onto a precision milled corner cube,[4] here we also show that the misalignment can be corrected with front optics. While the off-the-shelf optics shown here is quite bulky, it was done to illustrate that the need for a precision milled corner cube can be avoided. In future work it will be determined if a combination of more advanced front optics and a free-standing PCB retromodulator can be a better solution in terms of weight, cost, etc., than using a precision corner cube.

5 Demonstration of Corrective Front Optics for the Imperfect Retroreflector

To design a correction system, this IRR was modeled in LightTools® by Optical Research Associates (ORA®, Pasadena, California), which is a 3-D ray tracing software. The source and detector was set at a distance of 2.5 m from the IRR. The horizontal and vertical rotation of the IRR results in the spots moving around the axis, with no optical power being retroreflected back to the detector. Any correction system that is introduced will require the multiple diverging beams to be redirected back to the optical axis, as shown schematically in Fig. 11. It should also be tolerant to the

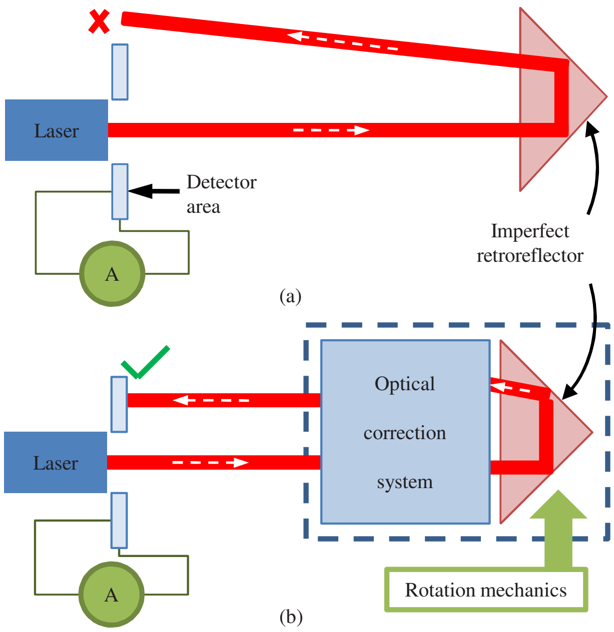

Fig. 11 Schematic showing the retroreflection system (a) without and (b) with the optical correction system.

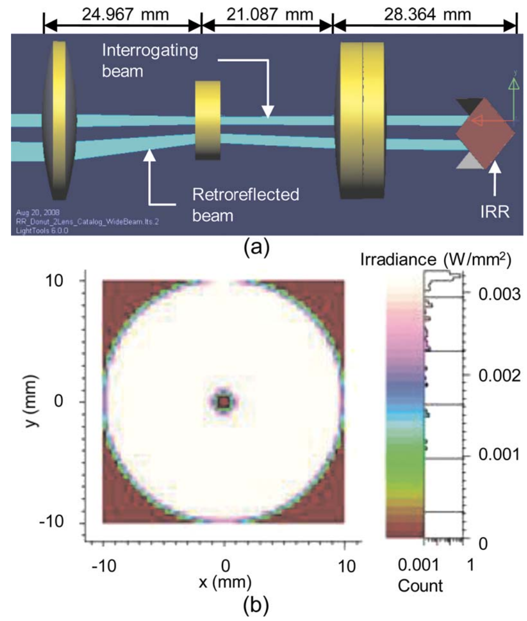

Fig. 12 (a) The triple-lens correction system model from LightTools®. The optimal separation (in millimeters) between the lenses and imperfect retroreflector are indicated for an interrogation distance of 2.5 m between the source/detector and the retroreflector. (b) Spot observed on the annular detector ($P_{detector}$=0.975 W, P_{launch}=1 W). The detector has an outer and inner radius of 10 and 1 mm, respectively.

rotation of the IRR that it is designed for to allow for imperfect alignment in the applications such as military identification systems on the battlefield.

An annular detector with an inner and outer radius of 1 and 10 mm, respectively, is used in the theoretical modeling of the correction system. The correction system must be designed for an IRR that is offset from the optical axis, so that the interrogating beam hits one of the faces and not the vertex of the module. During the PCB assembly, gaps may be introduced between reflective faces due to imperfect alignment, resulting in the leakage of the interrogating laser beam. Also, the active area of the modulators in a MRR does not typically extend to the edge of the device. Hence, any light incident along the edges of the devices is effectively "wasted" and the CR is significantly diminished.

The optical correction system designed and optimized for high efficiency operation at a distance of 2.5 m is shown in Fig. 12(a). It redirects the diverging retroreflected beam back to the optical axis to achieve true retroreflection. A very high theoretical efficiency of about 97.5% is achieved. Figure 12(a) also indicates the optical separation between the three lenses and the IRR. The optimized correction system utilized the readily available catalog lenses NT08-016, NT08-034, and NT32-492 (biconvex, biconcave, and achromat, respectively) from Edmund Optics®, (Barrington, New Jersey). The retroreflected beam evenly illuminates the annular detector, as shown in Fig. 12(b). The dependence of optical power incident on the detector with the horizontal and vertical rotation of the module is shown in Fig. 13. A FWHM angle of 19.13 and 23.48 deg in the horizontal and vertical rotational directions, respectively, is calculated.

The correction system was setup and tested using the experimental setup shown in Fig. 14. For the experimental validation of the corrected retroreflection, a circular-shaped detector was placed very close to the HeNe laser. A single retroreflected beam is shown illuminating the detector. The dependence of the detector photocurrent on the rotation of the IRR is shown in Fig. 15. The vertical angle (ϕ) could only be varied from −10 to +4.5 deg due to the limitation on the angular stage used. The experimental FWHM angle for vertical rotation is approximately 24.43 deg, which matches well with the theoretical prediction. However, the experimental FWHM angle for the horizontal (θ) rotation is approximately 15.46 deg. This slight deviation from the

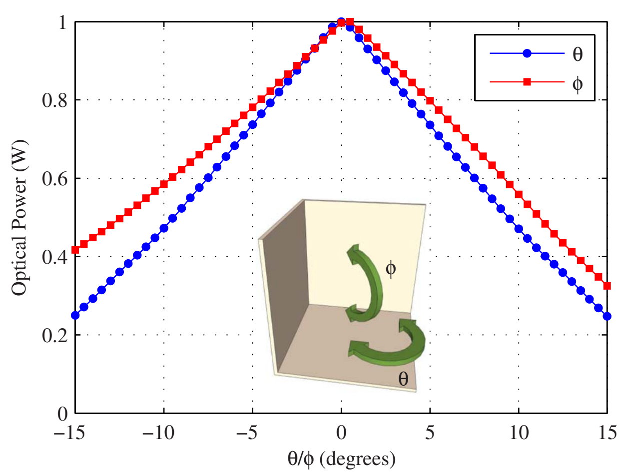

Fig. 13 Theoretical dependence of optical power retroreflected onto the detector by the triple-lens-corrected retroreflector module on the horizontal (θ) and vertical (ϕ) rotation of the module as indicated in the inset. A peak efficiency of about 97.5% is observed.

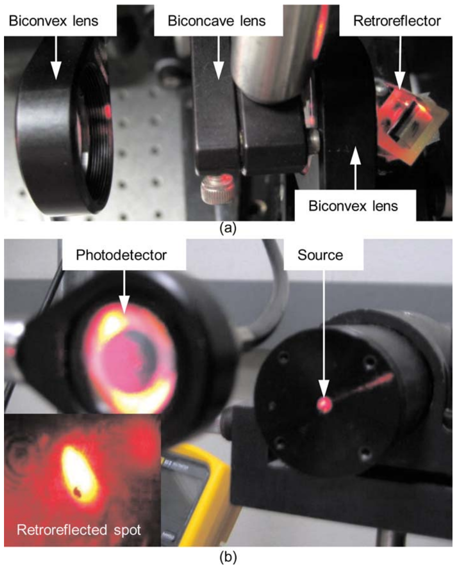

Fig. 14 (a) Experimental setup to test the correction system. (b) Also shown is the source-detector setup with the now retroreflected light illuminating the detector. The bottom-left inset shows the true retroreflected spot.

theoretical model is because we used a single laterally shifted circular-shaped detector instead of an annular detector.

The optical correction system proposed here utilized three lenses to correct for the angular misalignment of the three faces of the MRR. Thus, the effective length of the MRR is about 75 mm. However, from a system assembly as well as usability standpoint, a more compact correction system may be desirable. This may be possible by designing a custom triplet lens and optimizing the curvatures of the various lens interfaces to achieve true retroreflection from an imperfect retroreflector. In addition to resulting in a more compact system, using one component for optical correction greatly reduces the system complexity and relaxes the constraints on alignment during system assembly.

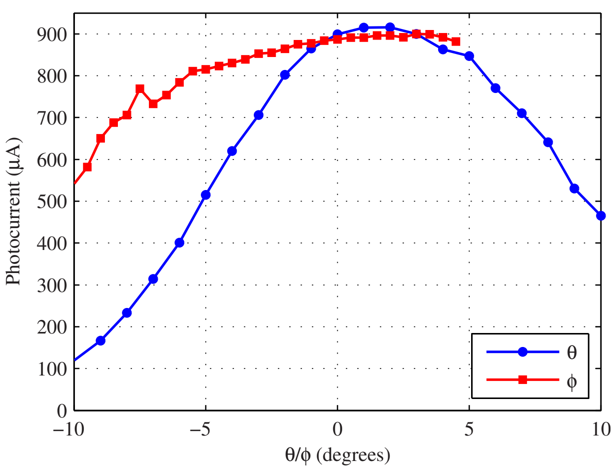

Fig. 15 Experimental result. Dependence of detector photocurrent on the horizontal (θ) and vertical (ϕ) rotation of the IRR.

6 Conclusion

In this work, we demonstrate the use of standard microelectronics packaging technology for the construction of a modulating retroreflector. The retroreflector is constructed using FR4. The module consists of three large-area InP-based multiple quantum well devices operating in the 1550-nm region, which are bonded on the three faces of the corner cube. The quantum well devices fabricated using MOCVD show lower defect density than similar devices fabricated using MBE. The assembled MRR showed a high CR of 8.23 dB at 20-V reverse bias. The free-standing printed circuit board MRR shown here had angular misalignments of ± 0.5 deg, and this is shown to be insufficient tolerance for long-distance retrocommunication. While mounting the PCBs on a precision corner cube is a known solution, an optical correction system to correct for the alignment errors in the free-standing printed circuit board MRR is designed and demonstrated.

Acknowledgment

This work was supported by the Defense Advanced Research Projects Agency Microsystems Technology Office (DARPA-MTO), under the grant HR0011-07-1-0039 (approved for Public Release, Distribution Unlimited).

References

1. G. C. Gilbreath, W. S. Rabinovich, T. J. Meehan, M. J. Vilcheck, R. Mahon, R. Burris, M. Ferraro, I. Sokolsky, J. A. Vasquez, C. S. Bovais, K. Cochrell, K. C. Goins, R. Barbehenn, D. S. Katzer, K. Ikossi-Anastasiou, and Marcos J. Montes, "Large-aperture multiple quantum well modulating retroreflector for free-space optical data transfer on unmanned aerial vehicles," *Opt. Eng.* **40**(7), 1348–1356 (2001).
2. A. C. Nicholas, G. C. Gilbreath, S. E. Thonnard, R. Kessel, R. Lucke, and C. P. Sillman, "The atmospheric neutral density experiment (ANDE) and modulating retroreflector in space (MODRAS): combined flight experiments for the space test program," *Proc. SPIE* **4884**, 49–58 (2003).
3. M. Plett, W. S. Rabinovich, R. Mahon, M. S. Ferraro, P. G. Goetz, C. I. Moore, and W. Freeman, "Free-space optical communication link across 16 kilometers over the Chesapeake Bay to a modulated retroreflector array," *Opt. Eng.* **47**(4), 045001 (2008).
4. T. K. Chan and J. E. Ford, "Retroreflecting optical modulator using an MEMS deformable micromirror array," *J. Lightwave Technol.* **24**(1), 516–525 (2006).
5. N. S. Prasad and A. R. Geiger, "Remote sensing of propane and methane by means of a differential absorption lidar by topographic reflection," *Opt. Eng.* **35**(4), 1105–1111 (1996).
6. D. H. Parker, M. A. Goldman, B. Radcliff, and J. W. Shelton, "Attenuated retroreflectors for electronic distance measurement," *Opt. Eng.* **45**(7), 073605 (2006).
7. S. P. Griggs, M. B. Mark, and B. J. Feldman, "Dynamic optical tags," *Proc. SPIE* **5441**, 151–160 (2004).
8. J. Blau, "Car talk," *IEEE Spectrum* **45**(10), 16 (2008).
9. J. N. Mait, M. W. Haney, K. W. Goossen, and M. P. Christensen, "Shedding light on the battlefield—tactical applications of photonic technology," *Defense Technol.*, Paper 7 (2004), http://www.ndu.edu/CTNSP/Def_Tech/DPT7%20Photonics.pdf.
10. C. Luo and K. W. Goossen, "Free-space optical link by microelectromechanical system array and corner cube retroreflector," *IEEE Photonics Technol. Lett.* **17**(6), 1316–1318 (2005).
11. C. Luo and K. W. Goossen, "Optical microelectromechanical system array for free-space retrocommunication," *IEEE Photonics Technol. Lett.* **16**(9), 2045–2047 (2004).
12. D. Pederson and O. Solgaard, "Free space communication link using a grating light modulator," *Sens. Actuators, A* **A83**, 6-10 (2000).
13. C. M. Swenson, C. A. Steed, I. A. DeLaRue, and R. Q. Fugate, "Low power FLC-based retromodulator communications systems," *Proc. SPIE* **2990**, 296–310 (1997).
14. B. Perezhki, S. M. Lord, and J. S. Harris, "Electroabsorptive modulators in InGaAs/AlGaAs," *Appl. Phys. Lett.* **59**, 888–890 (1991).

15. K. W. Goossen, J. E. Cunningham, W. Y. Jan, and R. Leibenguth, "On the operational and manufacturing tolerances of GaAs–AlAs MQW modulators," *IEEE J. Quantum Electron.* **34**(3), 431–438 (1998).
16. K. W. Goossen and D. W. Prather, "Fabrication and yield of large-area quantum-well modulators," *IEEE Photonics Technol. Lett.* **19**(24), 2054–2056 (2007).
17. J. M. Fastenau, D. Lubyshev, Y. Wu, C. Doss, and W. K. Liu, "Comparative studies of the epireadiness of 4 in. InP substrates for molecular-beam epitaxy growth," *J. Vac. Sci. Technol. B* **23**(3), 1262–1266 (2005).
18. "EpiHBT™ InP wafers," see http://www.epiworks.com/products/images/EpiHBT_InP.pdf.
19. Q. Wang, S. Junique, D. Agren, B. Noharet, and J. Y. Andersson, "Fabry-Pérot electroabsorption modulators for high-speed free-space optical communication," *IEEE Photonics Technol. Lett.* **16**(6), 1471–1473 (2004).
20. K. Ikossi, W. S. Rabinovich, D. S. Katzer, S. C. Binari, J. Mittereder, and P. G. Goetz, "Multiple quantum well PIN optoelectronic devices and a method of restoring failed device characteristics," *Microelectron. Reliab.* **42**(7), 1021–1028 (2002).

Rohit Nair received the BE degree in electronics and telecommunication engineering from Pune University, India, in 2002, and the MS degree in electrical and computer engineering from the University of Delaware, Newark, in 2007, where he is currently working toward the PhD degree. His research focuses on optical interconnects using quantum-well-based devices for intrachip, interchip, and board-level optical interconnects, as well as long range free-space optical interconnects.

Michael E. Teitelbaum received a BS in materials science and engineering from the University of Maryland, College Park, and a PhD in electrical engineering at the University of Delware, Newark. His experience is in optoelectronic devices and fabrication. Currently, his postdoctoral research at the University of Delaware is focused on free space optical interconnects and superluminescent devices for focal plane arrays.

Keith W. Goossen has 20 years professional experience in the fields of optoelectronics and optical fiber communication, resulting in more than 100 refereed journal papers, numerous invited talks and conference proceedings, and 80 patents. After receiving his PhD from Princeton University in 1988, he went to Bell Laboratories, where he invented and demonstrated a micromechanical optical modulator, which was used for broadband fiber-to-the-home networks and dynamic management of WDM networks. He also invented and demonstrated flip-chip bonding techniques for integrating electronic and photonic chips, which resulted in chips capable of processing up to a terabit/second of data. He cofounded Aralight, Incorporated as a chief scientist in 2000 to commercialize this technology for optical backplane applications, and in 2002, helped guide the engineering development to a full product demonstration of 90-Gbit/s optical modules. He joined the University of Delaware as an associate professor in 2002 in the Department of Electrical and Computer Engineering, where his work has included optical MEMS for free space communication, embedding of optical fiber networks in composite materials, and packaging of multielement high efficiency solar cells.